ANALYSIS OF PROPELLER SLIPSTREAM FIELD

Dieqian Wang, Ingemar Lindblad, Peter Eliasson
The Aeronautical Research Institute of Sweden, FFA
P.O. Box 11021, S-161 11 Bromma, Sweden

Abstract

A time averaged actuator disc model for steady state computations has been created based on Euler equations solver results of a propeller. The actuator disc model has been used in the Euler solver to show propeller slipstream field properties. The comparisons of slipstream field properties between the actuator disc model results and the propeller results from Euler solver in blade fixed Cartesian coordinates will show on the paper. It shows how this actuator disc steady state solutions is related to the time-averaged solutions from the time-dependent solutions in the Euler equations solver. The comparisons reveal the physical essential for the different propeller models. It explains how the time averaged actuator disc model can present, to a certain extent, such a complicated time dependent propeller slipstream field. It reveals also the main feature of the propeller slipstream field.

Summary

There has been continuing interest in propeller driven aircraft. The predictions of how the propeller slipstream influences the flow field are very important in the design phase of a new propeller driven aircraft. The flow over the nacelle, the wing and the stabilizer is affected considerably by a propeller. Detailed knowledge of the propeller slipstream and then the propeller model are important for the analysis the field of an aircraft. The flow field of a propeller is time-dependent and periodic. The time-dependent calculations around a full aircraft configuration with propeller on are still prohibitive. Therefore influence of the propeller is approximated by a time-average actuator disc model, which is widely used in the recent Euler solvers. In these paper momentum-blade element approximation or experimental data from an isolated propeller test are then used to set the forces boundary conditions at the disc to simulate the power loading of the propeller.

The experimental methods may be used to a degree. It is difficult and costly to develop and run model engines powerful enough in the wind tunnel test, especially at realistic cruise Mach numbers. The momentum-blade element approximation at least is doubtful under the conditions which are close to the cruise Mach number or transonic Mach number. However, at present, computational methods e.g. Euler solvers are best suited to provide the detailed knowledge of the flow essential to arrive at a superior design in a cost effective manner.

The data at the disc to simulate the power loading of the propeller, this simplification of the propeller effect is to compute a steady state solution by introducing the time-averaged propeller forces over one period. However, it is not known how this steady state solution is related to the time-averaged one of the time-dependent solution. The assumption is that the solutions are close. However, this is only verified in comparisons with windtunnel experiments where the time-averaged data are recorded.

Therefore, the task in the paper is to show how this steady state disc model solution is related to the time-averaged solution of the time-dependent solution from a propeller within Euler solver, in order to reveal the physical essential for the different propeller models. And then we will see why the time averaged actuator disc model can present, to a certain extent, such a complicated time dependent propeller slipstream field.

In the paper, it analyses the propeller slipstream field by solving the Euler equations in blade fixed Cartesian coordinates in a conservative finite volume algorithm and sets disc model based on this Euler equations solutions. The study reveals the feature of the propeller slipstream field. The comparisons between them consolidate the the time averaged actuator disc model idea and support a more elaborate approximation disc model in the cost effective manner. Moreover, the paper also presents the influence of the grid resolution and numerical parameters.

Numerical Method

Euler Equations

The real propeller calculations were performed by solving the Euler equations in a rotating frame of reference, when a steady rotation ω is imposed on the reference system. The Euler equations can be written in integral form as

$$\frac{\partial}{\partial t}\int\int\int_{\Omega}\overline{U}d\Omega+\int\int_{\partial\Omega}\overline{\mathbf{F}}(\overline{U})\cdot\mathbf{n}dS+\int\int\int_{\Omega}\overline{S}(\overline{U})d\Omega=0, \quad (1)$$

where

$$\overline{U}=\begin{pmatrix}\rho\\ \rho u\\ \rho v\\ \rho w\\ \rho E_r\end{pmatrix},\quad \overline{\mathbf{F}}(\overline{U})=\begin{pmatrix}\rho\mathbf{u}\\ \rho u\mathbf{u}+p\mathbf{i}\\ \rho v\mathbf{u}+p\mathbf{j}\\ \rho w\mathbf{u}+p\mathbf{k}\\ (\rho E_r+p)\mathbf{u}\end{pmatrix},$$

$$\overline{S}(\overline{U})=\begin{pmatrix}0\\ -\rho(\omega^2x+2\omega v)\\ -\rho(\omega^2y-2\omega u)\\ 0\\ 0\end{pmatrix}.$$

and E_r is defined by

$$E_r=\frac{1}{\gamma-1}\frac{p}{\rho}+\frac{\mathbf{u}\cdot\mathbf{u}-\omega^2(x^2+y^2)}{2}.$$

where ρ is the density, u, v, w are the Cartesian velocity components, $\mathbf{u}$ is the velocity, p is the pressure, and γ is the gas constant.

If the actuator disc model are used, then $\omega = 0$ in the Euler equations (1), i.e. without the third term on the left side in equations (1). This equations are satisfied everywhere in the interior of the computational domain, except for the propeller region. And over the propeller region, the terms regarding to the external forces generated by the propeller should be added on the rightside of the equations, insted of zero.

The governing equations are solved numerically using a conservative finite volume algorithm [1][2]. The code EURANUS [3] which is a general purpose code developed for the European Space Agency has been used for the calculations. The algorithm is based on a cell-centered finite volume approximation using structured meshes in Cartesian coordinates. The numerical flux at a cell face is computed via the central interpolation.

The source terms representing the rotational effects are computed by multiplying the appropriate cell average quantities by the cell volume. This spatial discretization is equivalent to a centered difference approximation of the spatial derivatives and is second order accurate on a uniform Cartesian grid [4].

In the disc model calculations, the equations at disc are treated as a special block connected conditions which has been implemented in EURANUS recently.

Disc Model

In the disc model, the propeller is replaced by a disc which is located at a layer of grid. The Euler equations including external forces generated by the propeller are

$$\frac{\partial\rho}{\partial t}+\frac{\partial(\rho u)}{\partial x}+\frac{\partial(\rho v)}{\partial y}+\frac{\partial(\rho w)}{\partial z}=0$$

$$\frac{\partial(\rho u)}{\partial t}+\frac{\partial(\rho u^2)}{\partial x}+\frac{\partial(\rho uv)}{\partial y}+\frac{\partial(\rho uw)}{\partial z}+\frac{\partial p}{\partial x}=f_x$$

$$\frac{\partial(\rho v)}{\partial t}+\frac{\partial(\rho vu)}{\partial x}+\frac{\partial(\rho v^2)}{\partial y}+\frac{\partial(\rho vw)}{\partial z}+\frac{\partial p}{\partial y}=f_y \quad (2)$$

$$\frac{\partial(\rho w)}{\partial t}+\frac{\partial(\rho wu)}{\partial x}+\frac{\partial(\rho wv)}{\partial y}+\frac{\partial(\rho w^2)}{\partial z}+\frac{\partial p}{\partial z}=f_z$$

$$\frac{\partial(\rho E)}{\partial t}+\frac{\partial(\rho Eu+up)}{\partial x}+\frac{\partial(\rho Ev+vp)}{\partial y}+\frac{\partial(\rho Ew+wp)}{\partial z}=Q$$

where E is the total energy
$Q = uf_x + vf_y + wf_z$
and f_x, f_y, f_z are different from zero only on the disc.

If the indices 1 and 2 denote the values at the upstream and downstream side of the disc respectively, propeller axis direction is $\mathbf{n} = (\mathbf{n_x}, \mathbf{n_y}, \mathbf{n_z})$ and velocity in the normal direction on the disc is $U = \mathbf{u}\cdot\mathbf{n}$.

The conditions at the disc are

$$(\rho U)_1=(\rho U)_2$$

$$(\rho Uu)_1+p_1n_x+f_x=(\rho Uu)_2+p_2n_x$$

$$(\rho Uv)_1+p_1n_y+f_y=(\rho Uv)_2+p_2n_y \quad (3)$$

$$(\rho Uw)_1+p_1n_z+f_z=(\rho Uw)_2+p_2n_z$$

$$[\rho U(E+p/\rho)]_1+Q=[\rho U(E+p/\rho)]_2$$

In subsonic flow four characteristics enter the disc from the upstream side and one characteristic from the downstream side. Therefore for stability the mass flux in the disc normal direction is taken from the downstream cell and the other quantities in Eqs.(3) are taken from the upstream cell. In the numerical implementation, the Eqs.(3) are treated as a special block connected condition. Solving the Eqs.(3) explicitly according to the per area forces (f_x,f_y,f_z) and neighbour cell center variables, the variables at disc for both two sides

are updated and then the dummy cell variables are updated again by the extrapolation in order to set such jump condition at the disc. This is somewhat similar to [5] and [6].

The forces per area on the disc are defined from the load distribution on the propeller blade, the solution from Euler equations in the rotating frame of reference system Eqs.(1). The steady disc model is a time-averaged disc model. Integrate the load during one period to get time averaged load per length along the propeller span. And then distribute the load over the disc area according to the grid in the disc calculation to keep the same time averaged load per length along the span.

Numerical Results

The case has been chosen to investegate the propeller slipstream field, the propeller is an unswept 4 bladed of radius $r_p = 1.6m$ and chord 0.2 m at all radii. The airfoil sections are of the 4 digit symmetric NACA series. The blad is twisted around the pich change axis. The flight condition is Mach number 0.5 and advance ratio is 0.7808. The propeller is mounted on a sting with a spinner on the top. The propeller rotation is in the x-axis direction and incoming flow is opposite to the x-axis.

The grid is generated by the method of transfinite interpolation [7]. The different sizes for far field and finer or coarser grids have been tested for proreller and disc model calculations.

The results are presented here mainly the comparisons between the time averaged results of propeller calculations and the results of the time-averaged disc model.

Fig.1 is the propeller velocity field survey, where close to the propeller tip in radial position about $r/r_p = 0.995$, at downstream of the propeller in different x positions. They are $-0.1485; -0.2; -0.4; -1.0; -2.0; -3.0$; and -5.0. The results are from Euler solver in blade fixed Cartesian coordinates during one time period. The time-dependent and periodic character can be seen clearly whole the way down to the far field. In these figures, the abscissa is a measure of time and figures are plotted during one time period, the ordinate values are disturbance velocity components in circumferential (solid line), radial (dashed line) and x (fine dashed line) directions respectively, but they have been normalized by the absolut free stream velocity, V_φ/V_∞, V_r/V_∞, $(V_x - V_\infty)/V_\infty$. The peak values become smaller and the time dependent feature become somewhat smoother going downstream. The interesting feature is that all of the time-averaged values have rather good agreement with the results from disc calculations. The propeller velocity field survey outside of propeller tip but close to the tip has the same characteristic as shown in Fig.1. At all of the radial positions, except near the propeller tip downstream , the time dependent feature smooth out quickly away from the propeller rotating surface about a order of a propeller chord length.

The comparison between the time averaged results of propeller calculations and the results of the time-averaged disc model can been seen in Fig.2. Fig.3 and Fig.4. The good agreement between the time averaged results of propeller calculations and the results of the disc model calculations appears at all radial positions as one can see in Fig.2, Fig.3 and Fig.4.

In Fig.2 they are the comparisons between the time averaged results of propeller calculations and the results of the disc model at $r/r_p = 0.6$, where it is at about in the middle of the propeller in the radial direction. The positive x value is corresponding to the upstream and the negative is corresponding to the downstream. In Fig.2a is circumferential velocity component V_φ/V_∞ versus x. In Fig.2b is radial velocity component V_r/V_∞ versus x. In Fig.2c is velocity component in x direction V_x/V_∞ versus x. And in Fig.2d is $(p - p_\infty)/p_\infty$ versus x.

Fig.3 is the comparisons between the time averaged results of propeller calculations and the results of the disc model at $x = -0.1485$, where it is just behind the propeller blad downstream. In Fig.3a is V_φ/V_∞ versus r/r_p. In Fig.3b is V_r/V_∞ versus r/r_p. In Fig.3c is V_x/V_∞ versus r/r_p. And in Fig.3d is $(p - p_\infty)/p_\infty$ versus r/r_p.

And in Fig.4 it is the comparisons between the time averaged results of propeller calculations and the results of the disc model at $x = -3$, much more further downstream compared to Fig.3.

In the figures we try to use different scale for plotting in order to see the deviation between the two models. In Fig.3 one can see rather larger deviation between the two models for the small r/r_p. Those deviations are caused by the different sting geometry in the two models calculations. In the disc model the sting after the position at trailing edge of the propeller root section the radius keeps the same. And in the propeller calculation the sting radius keeps increasing linearly whole way downstream. The difference in geometry of sting certainly makes larger redial velocity, smaller velocity in x direction and larger static pressure in the propeller calculation results. Because this kind of deviations does not appear in another coarser grid in the propeller calculation.

All of the pictures mentioned abobe are the results from the finest grid 289*65*65 in the propeller calculation and grid 257*2*97 in the disc calculation.

The grid fineness and fourth-order artifical viscosity do not effect the results in the disc calculations very much in this example. It is invisible deviation from plotting (in the reasonable scale, of cause) in all of the variables except in V_φ. Here in Fig.5 it shows the influences from grid fineness and fourth-order artifical

viscosity on V_φ versus r/r_p at $x = -0.1458$ and Fig.6 is at $x = -3$. In Fig.7 it shows the influences from the grid fineness and fourth-order artifical viscosity on V_φ versus x at radial positions $r/r_p = 0.2525$ and $r/r_p = 0.991$. In Fig.5, Fig.6 and Fig.7 the dashed lines are from the finest grid results with the value of the scaled fourth-order artifical viscosity, which is recommended in EURANS for the general case calculation. The solid lines are from the finest grid results but half of value of the scaled fourth-order artifical viscosity, which is used in dashed lines case. And the fine dashed lines are the results for cocrser grid with lower artifical viscosity. From Fig.5, Fig.6 and Fig.7 the artifical viscosity have larger influence in the variatin of V_φ in the incoming flow direction and larger influence when V_φ is larger. So the artifitial viscosity might have larger influence under the high loading case.

In the propeller calculations, no considerable deviation was found in the results caused by the grid fineness.

From the numerical study we can see that the time-averaged disc model can describe the propeller field rather well in the time-averaged sense in the Euler method. And the time-averaged disc model certainly can not describe the tip vortex.

Conclusions

The numerical study given above has been shown how this steady state solution in the disc model is related to the time-averaged of the time-dependent solution in the Euler equations solver. It consolidates the time-averaged actuator disc model and it gives reliable and feasible way to set data base for the disc model calculation in a cost effective manner.

Propeller flow field is complicated and time dependent. Since in this study it has revealed that the time dependent feature appears strongly in the field where the region is very close to (in the order of the propeller chord length only in this example) the propeller rotating surface and propeller tip wake region only. The propeller tip wake almost keeps the same time dependent character as just behind the propeller. This makes it is possible to simulate the propeller by disc model in the steady calculations except any effect which is related to the tip vortex. More interesting thing is however, the time-averaged disc model results have so good agreement with the time averaged ones from propeller calculations. The grid fineness and far fild size do not influence considerablely the road distribution on the propeller blade. The load distribution from the propeller calculation is a good source to support the data base for the disc simulations.

This is a primary study. More study should be done.

References

(1) Jameson, A. and Baker, T.J. Solution of the Euler Equations for complex configurations, AIAA paper 83-1929CP

(2) Rizzi, A. and Eriksson, L.-E. Computation of Flow around Wings Based on the Euler Equations. J. Fluid Mechanics, 148,45-71, 1984

(3) Rizzi, A., Eliasson, P., Lindblad, I., Hirsch, Ch., Lacor, C. and Haeuser, J., The Engineering of Multiblock/Multigrid Software for Navier-Stokes Flows on Structured Meshes, Computers & Fluids, Vol. 22, No. 2/3, 1993, pp. 341-367.

(4) Lindblad, I., On the Resolution of the Nonlinear Near Field of a Single-Rotation Propfan with a Numerical Solution of the Euler Equations, AIAA-90-3995,1990

(5) Per Lotstedt, Properties of a Propeller Model in the Stationary Euler Equations, Proceedings of ECCOMAS, 1994

(6) N. J. Yu and H. C. Chen, Flow Simulations for Nacelle-Propeller Configurations Using Euler Equations, AIAA-84-2143

(7) Tysell, L and Hedman, S. G. Towards a general three-dimensional grid generation system, ICAS Paper 88-4.7.4.

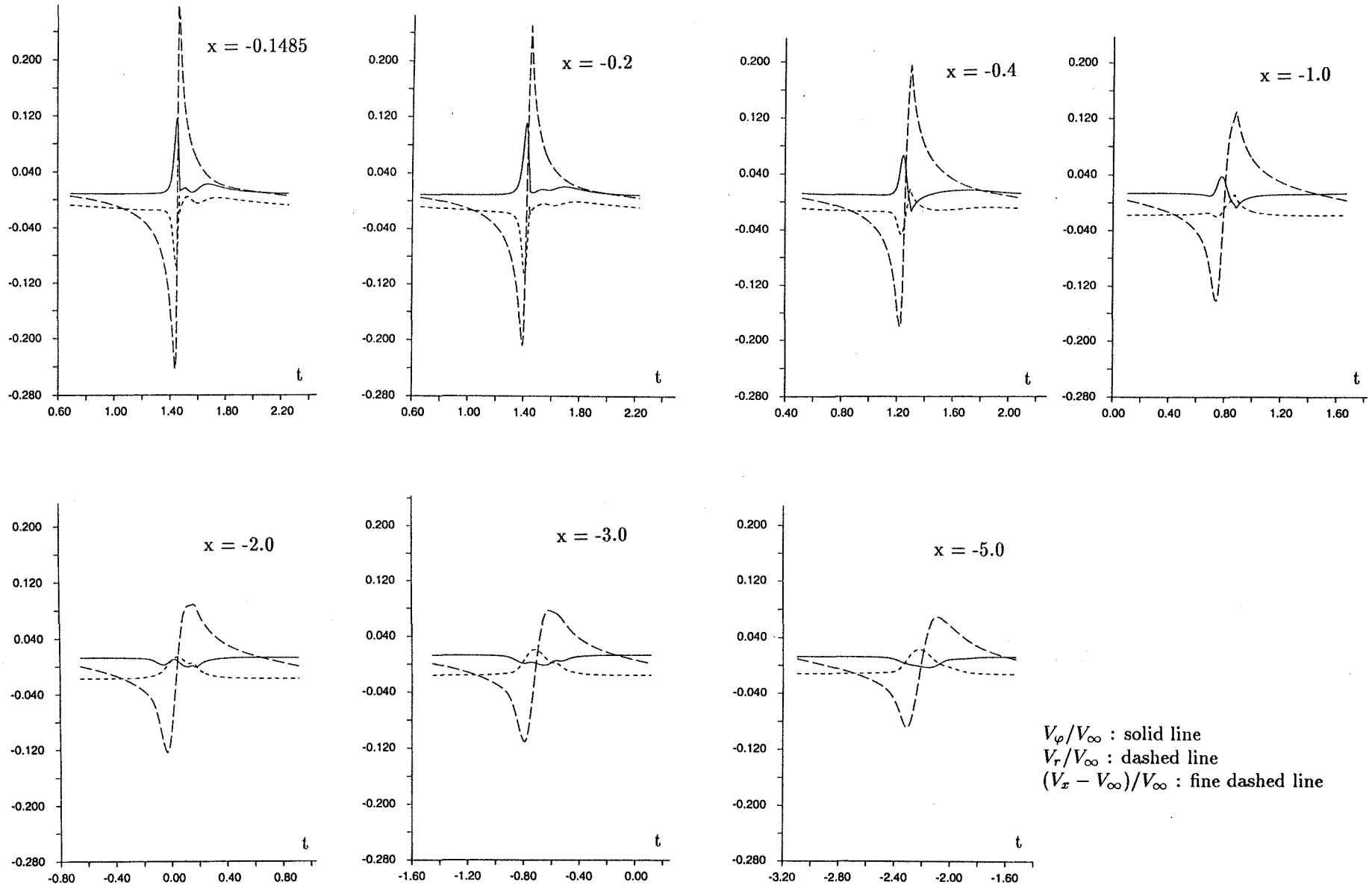

Fig.1 Propeller velocity field survey at $r/r_p = 0.995$.

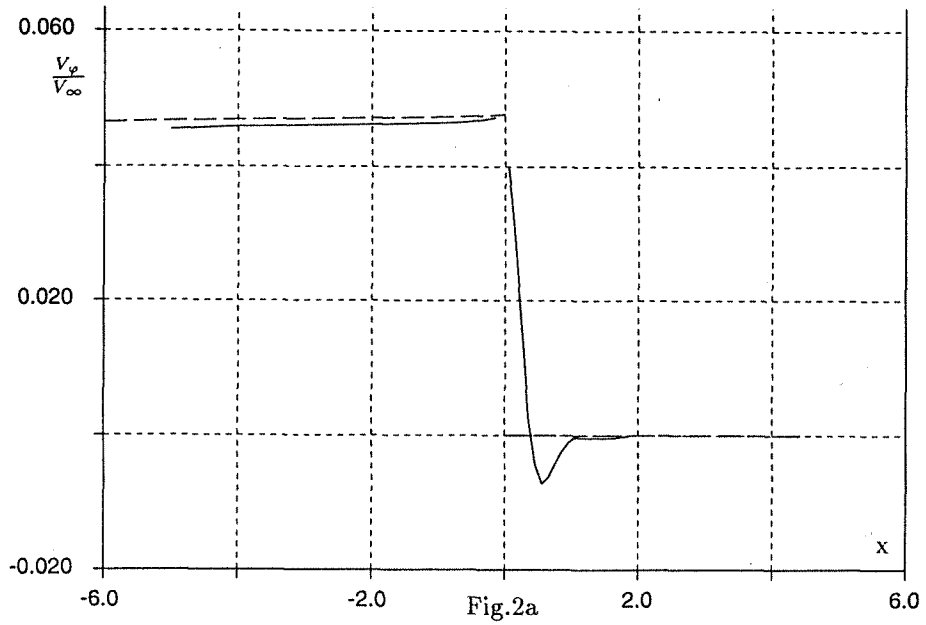

Fig.2a

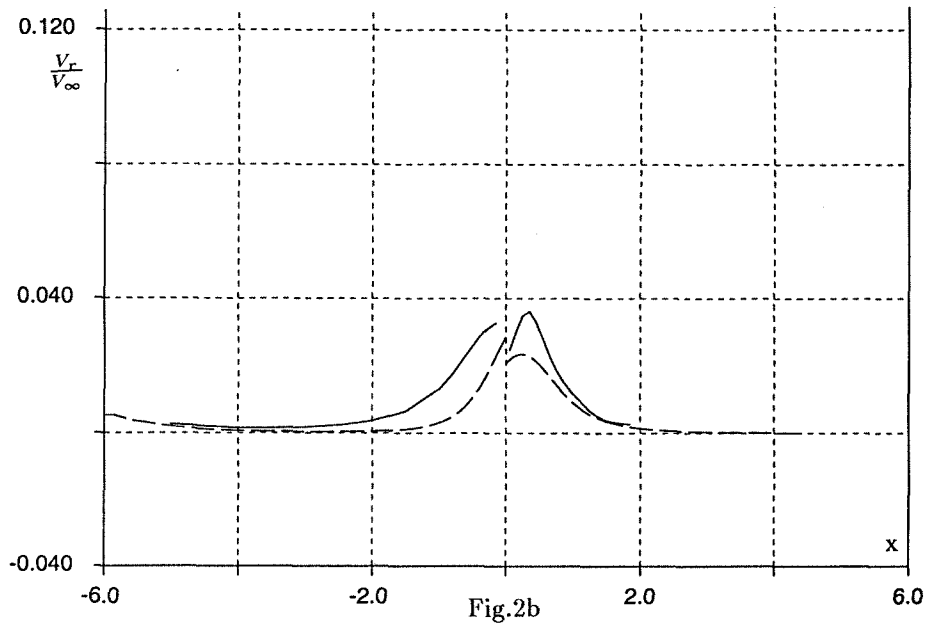

Fig.2b

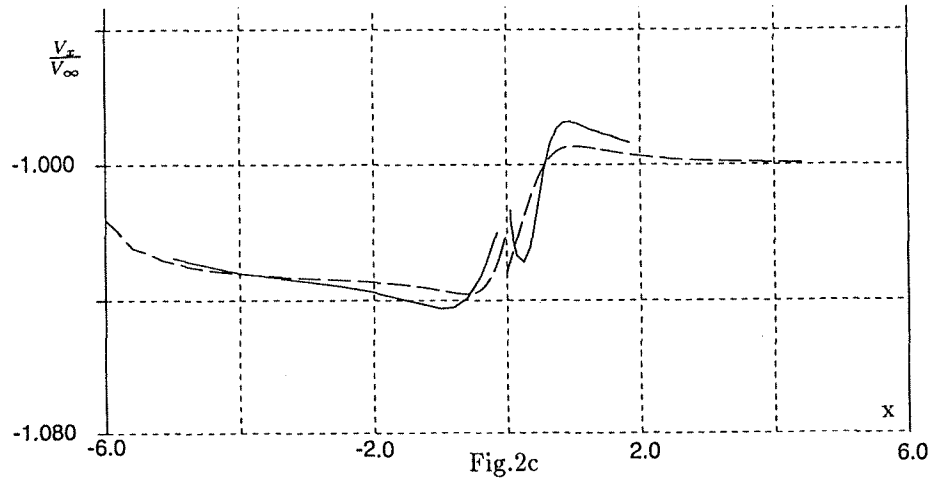

Fig.2c

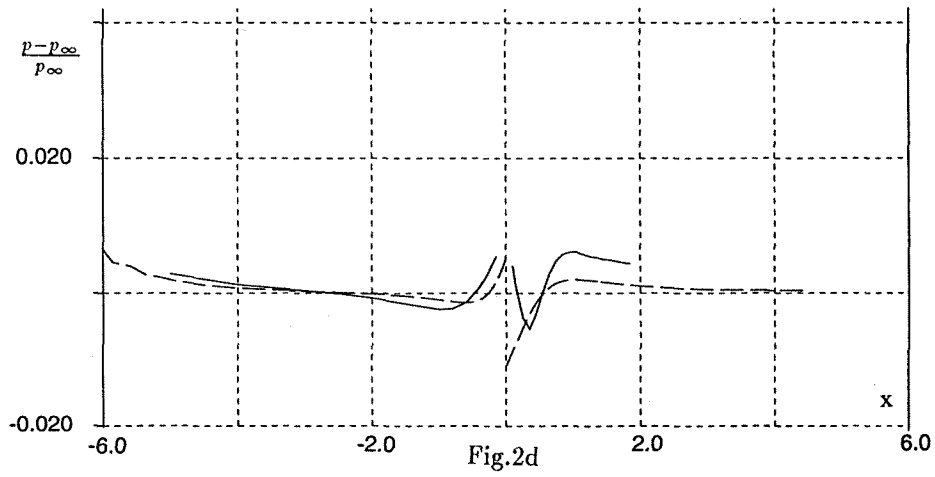

Fig.2d

Fig.2 Comparisons between the time averaged results of propeller (solid line) and disc model (dashed line) at $r/r_p = 0.6$.

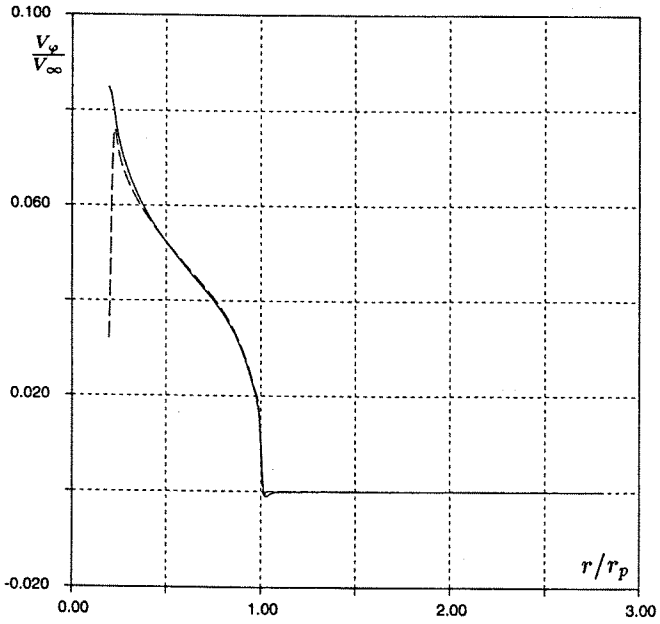

Fig.3a

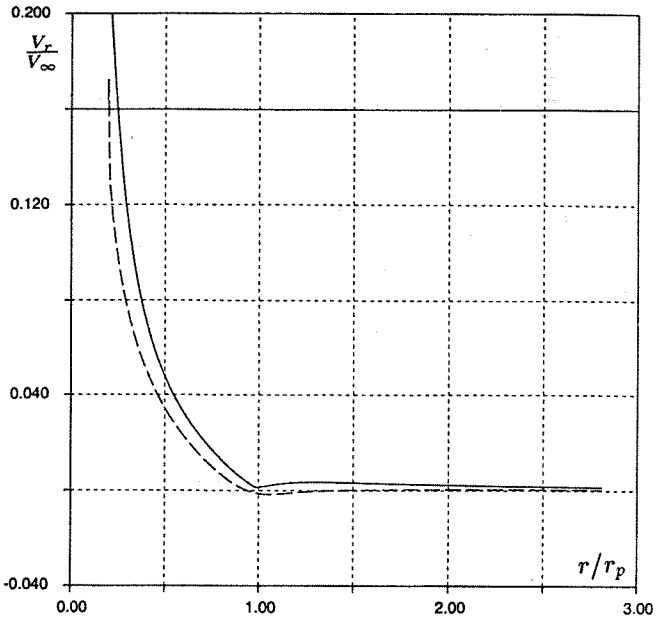

Fig.3b

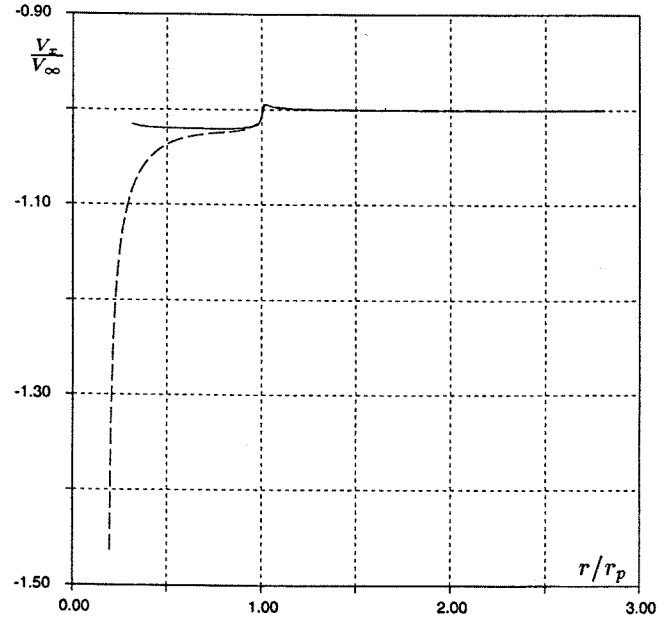

Fig.3c

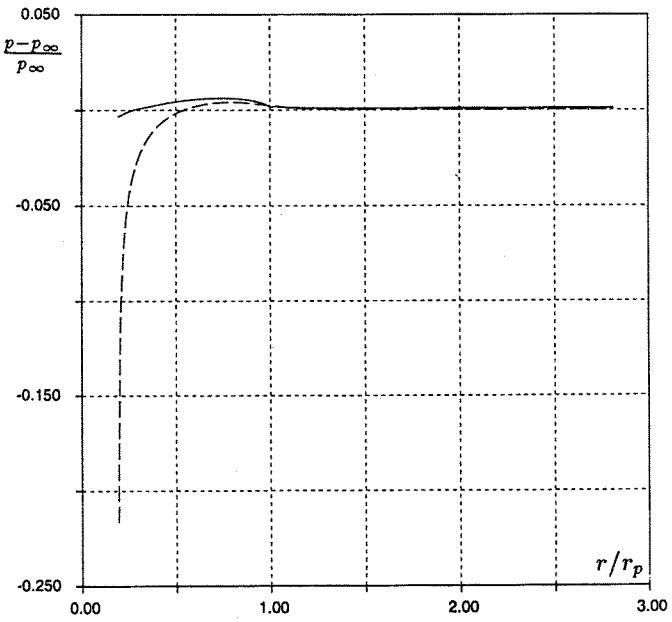

Fig.3d

Fig.3 Comparisons between the time averaged results of propeller (solid line) and disc model (dashed line) at $x = -0.1485$ (just behind the propeller).

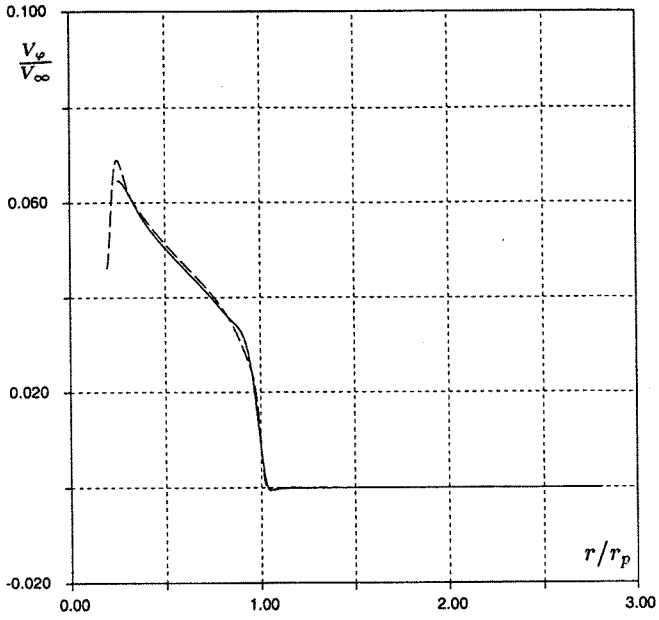

Fig.4a

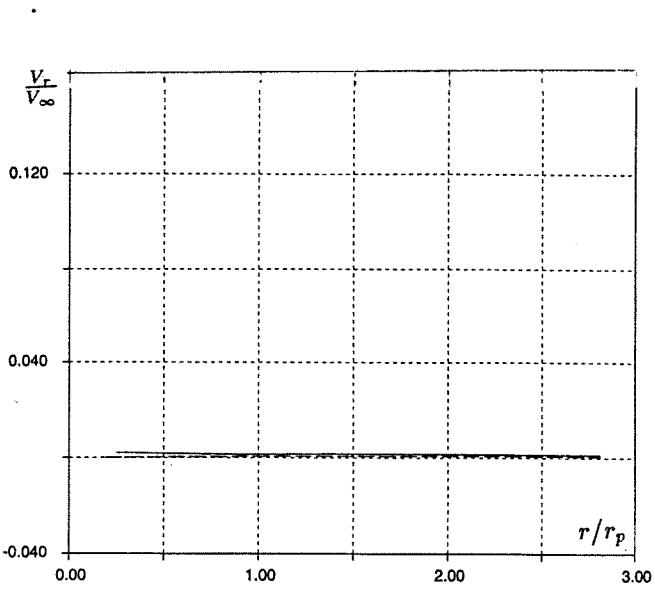

Fig.4b

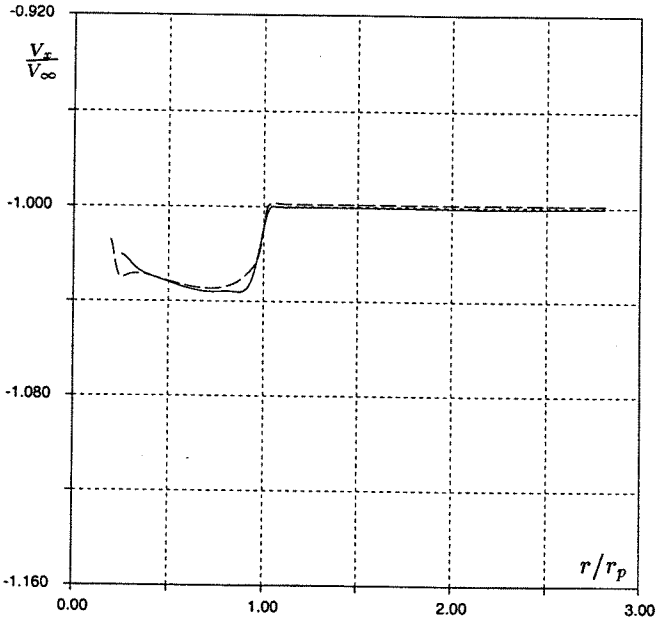

Fig.4c

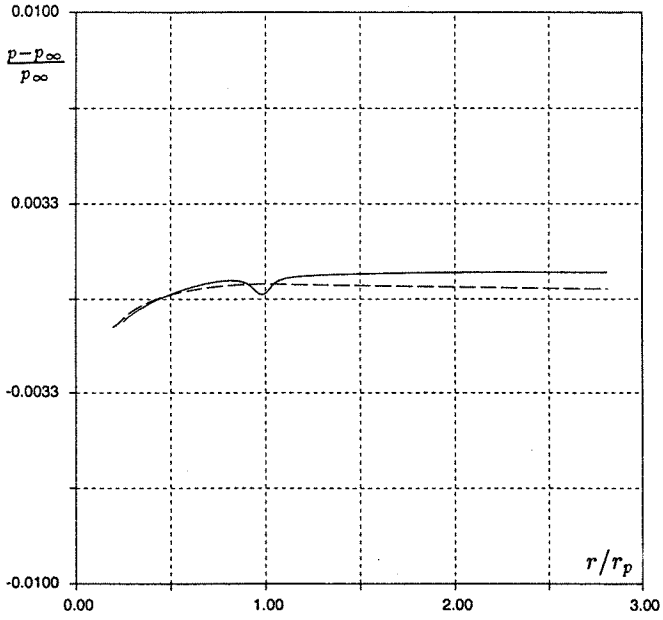

Fig.4d

Fig.4 Comparisons between the time averaged results of propeller (solid line) and disc model (dashed line) at $x = -3$.

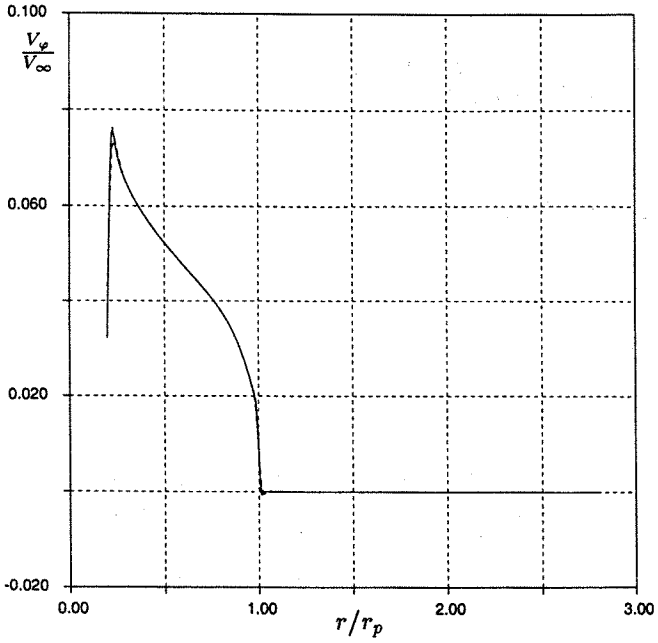

solid line : finest grid with lower viscosity
dashed line : finest grid with higher viscosity
fine dashed line : coarser grid with lower viscosity

Figure 5: Comparisons of grid fineness and viscosity at $x = -0.1458$.

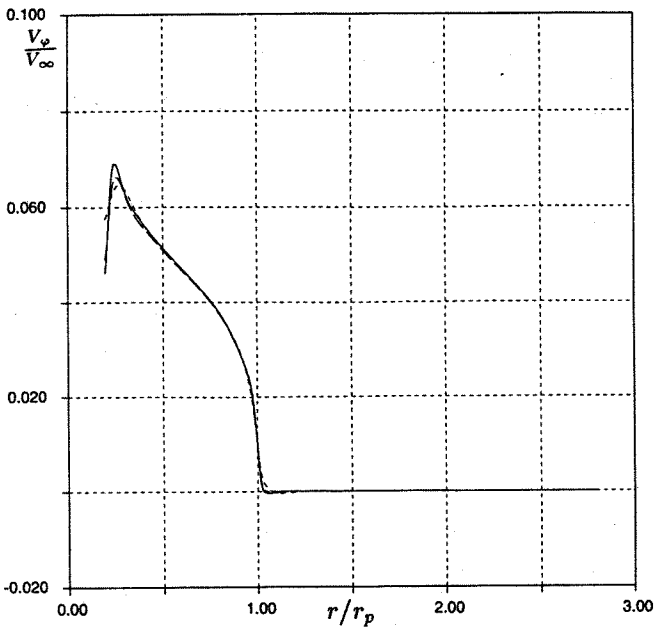

solid line : finest grid with lower viscosity
dashed line : finest grid with higher viscosity
fine dashed line : coarser grid with lower viscosity

Figure 6: Comparisons of grid fineness and viscosity at $x = -3$.

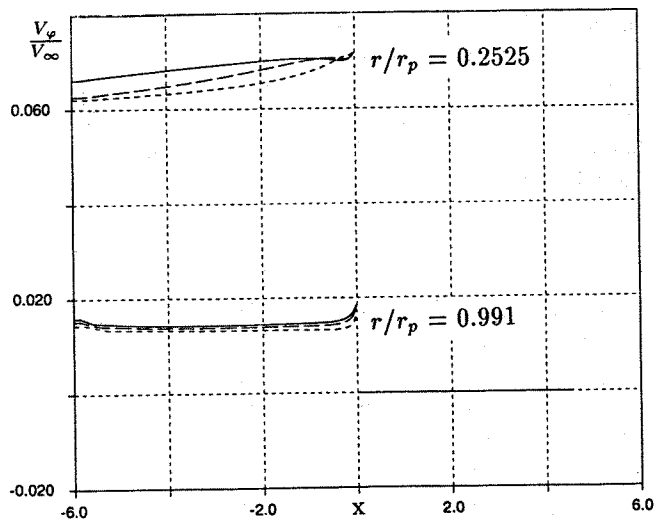

solid line : finest grid with lower viscosity
dashed line : finest grid with higher viscosity
fine dashed line : coarser grid with lower viscosity

Figure 7: Comparisons of grid fineness and viscosity at $r/r_p = 0.2525$ and $r/r_p = 0.991$.